Modeling and Stability Analysis of Islanded DC Microgrids Under Droop Control

André Pires Nóbrega Tahim, *Student Member, IEEE*, Daniel J. Pagano, *Member, IEEE*, Eduardo Lenz, *Student Member, IEEE*, and Vinicius Stramosk, *Student Member, IEEE*

***Abstract*—The stability of dc microgrids (MGs) depends on the control strategy adopted for each mode of operation. In an islanded operation mode, droop control is the basic method for bus voltage stabilization when there is no communication among the sources. In this paper, it is shown the consequences of droop implementation on the voltage stability of dc power systems, whose loads are active and nonlinear, e.g., constant power loads. The set of parallel sources and their corresponding transmission lines are modeled by an ideal voltage source in series with an equivalent resistance and inductance. This approximate model allows performing a nonlinear stability analysis to predict the system qualitative behavior due to the reduced number of differential equations. Additionally, nonlinear analysis provides analytical stability conditions as a function of the model parameters and it leads to a design guideline to build reliable (MGs) based on safe operating regions.**

***Index Terms*—Bifurcation analysis, constant power load (CPL), DC microgrid, droop control, nonlinear stability analysis.**

I. Introduction

DC networks are embedded in several autonomous systems from ships to notebooks, and have been gaining ground on energy distribution in the form of small dc microgrids (MGs). This resumption of dc power distribution is due to the ease of integration of renewable energy and the growing share of electronic loads in the system, which makes dc distribution an option to build more efficient systems [1], [2].

The main concern during the design of a dc MG is its stability, whose basic unit for stabilization and achieving the integration between loads and sources is the power converter [3], as illustrated in Fig 1. The power converters decouple loads and sources from disturbances and adjust the voltage levels required by each device in the network. In islanded dc MGs without communication, the system operates in a distributed control scheme where each unit has a controller whose decision is based on the available local variables [4]. In such context, the stability is commonly obtained by sources in parallel controlling the bus voltage cooperatively. A common practice to accomplish this without overloading some sources is to include a virtual resistance on the output of the sources power converter,

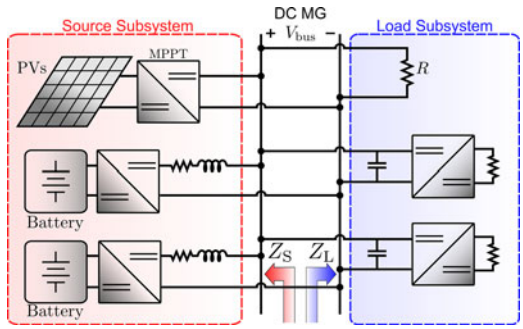

Fig. 1. Islanded dc microgrid with source and load subsystems highlighted.

a technique known as droop control [5]–[8]. Droop control increases the output resistance of each source, which makes them farther away from an ideal source, and consequently, there is greater interaction between sources and loads. Such interaction causes the stability of the bus voltage to be more dependent on the type of load coupled to the system. Additionally, dc MGs have nonlinear active loads with a constant power characteristic at their input terminals, which arise from tightly regulated point-of-load (POL) converters, commonly referred as constant power loads (CPLs) [9], [10].

Most of the dc stability analysis are linear and based on the Middlebrook and Cuk criterion [11], due to the ease to obtain the system open-loop gain knowing only the output impedance of the source Z_s subsystem and the input impedance of the load subsystem Z_L [12]–[14], as illustrated in Fig. 1. Since dc MGs have a high insertion of nonlinear loads (CPLs), such loads must be linearized in a voltage operating point to be able to use these methods. This linearization results in a model composed by a negative resistance in parallel with a current source [15], [16] that is suitable to local stability analysis, near to the voltage operating point. In such context, many researches have successfully addressed the instability problem of constant power loads using linear stability analysis [17]–[19]. However, a droop-controlled dc MGs is allowed to work on voltage levels away from the linearization point [20], [21], making the linear negative resistance model unsuitable to stability analysis for the entire range of possible voltages.

To overcome this problem, nonlinear stability analysis is used to predict the system's global qualitative behavior. Such approach models the POL converters with a constant power characteristic to any operation voltage using the ideal CPL model, which assumes that the input power of a POL converter is constant and equal to the power demanded by the load [22]–[25]. This model although conservative keeps the nonlinearities and it

Manuscript received May 26, 2014; revised August 6, 2014; accepted September 9, 2014. Date of publication September 24, 2014; date of current version March 5, 2015. This work was supported in part by the Coordination for the Improvement of Higher Education Personnel, Brazil. Recommended for publication by Associate Editor Y. W. Li.

The authors are with the Department of Automation and Systems, Federal University of Santa Catarina, Florianópolis, Brazil (e-mail: andre.tahim@posgrad.ufsc.br; daniel.pagano@ufsc.br; eduardo.lenz@posgrad.ufsc.br; vinicius.stramosk@posgrad.ufsc.br).

Color versions of one or more of the figures in this paper are available online at http://ieeexplore.ieee.org.

Digital Object Identifier 10.1109/TPEL.2014.2360171

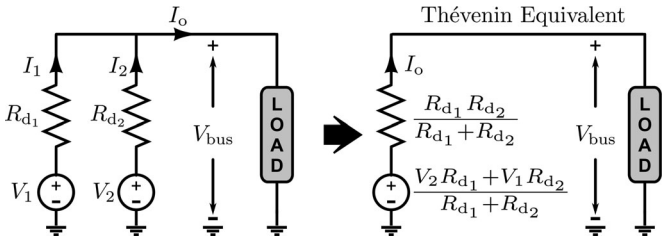

Fig. 2. Two sources in parallel feeding a common load and its Thévenin equivalent circuit.

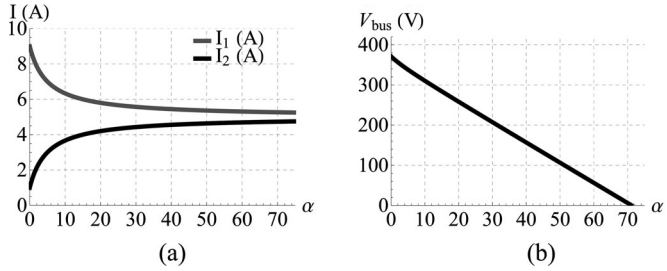

Fig. 3. Load sharing and bus voltage regulation using droop control; (a) Load sharing as the sources output resistances are increased by a factor of α. (b) Degradation of the bus voltage as α is increased.

is used in this paper. The major problem of the nonlinear stability analysis is the high number of differential equations, which makes it too complex or does not give much insight about how the interaction of the variables affect the stability. This paper has the following contributions:

1) An approximate model of the source subsystem with n parallel sources under droop control and their corresponding transmission lines by only one equivalent source and transmission line (see Section II). The equivalent model keeps the qualitative behavior of the system and reduces the n differential equations to only one, making the nonlinear stability analysis much less complex.
2) A relation among the total capacitance on the bus, the equivalent transmission line, and the maximum load that keeps the system stable for the entire range of possible bus voltages (see Section IV).
3) An explanation about the different types of system behaviors depending on the amount of resistance and constant power load using bifurcation analysis (see Section IV).

Section III is intended for system modeling and Sections V and VI present the simulation and experimental results, respectively.

II. Droop Control

The sources in a distributed control scheme operate cooperatively to regulate the bus voltage, but a load sharing problem arises, where each source must provide power to the load proportional to its power capacity. In such a context, load sharing is critical to avoid that some sources become overloaded, losing the reliability of distributed power systems.

To understand the difference between power supplied from parallel sources, a simplified circuit with two sources providing power to a given load is analyzed. The static analysis of such simplified circuit is done by modeling power sources as a voltage source V_i in series with an output droop resistance R_{d_i}, as illustrated in Fig. 2.

The difference in current supplied by each source in Fig. 2 is

$$I_1 - I_2 = \frac{2(V_1 - V_2)}{R_{d_1} + R_{d_2}} + \frac{(R_{d_2} - R_{d_1})}{R_{d_1} + R_{d_2}} I_o. \tag{1}$$

It can be noted from (1) that the difference in the current provided by each source is inversely proportional to $(R_{d_1} + R_{d_2})$. Therefore, as the output resistances R_{d_i} grow, the denominator of (1) increases, and consequently, load sharing is improved.

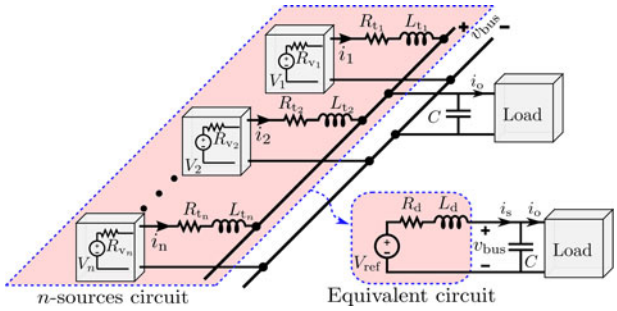

Fig. 4. DC MG composed by n sources in droop scheme (n-sources model) and the proposed equivalent circuit (equivalent model).

Thus, the main idea of the droop control is to increase the output resistance to reduce the difference between the currents.

It is depicted in Fig. 3(a), the current sharing of two power sources as the output resistances are increased gradually by a factor of α. The power sources feed a 10-A load with the same reference voltage ($V_1 = V_2$) and output resistances of $R_{d_1} = (1 + \alpha)$ and $R_{d_2} = (9 + \alpha)$.

It is noteworthy in Fig. 3(a) that the currents of each source get closer as the output resistances are increased. On the other hand, increasing the output resistances degrades the bus voltage regulation (V_{bus}) because the Thévenin resistance R_d is increased, as it becomes explicit by the equation obtained from the Thévenin equivalent circuit in Fig. 2

$$V_{\text{bus}} = \underbrace{\frac{V_1 R_{d_2} + V_2 R_{d_1}}{R_{d_1} + R_{d_2}}}_{V_{\text{ref}}} - \underbrace{\frac{R_{d_1} R_{d_2}}{R_{d_1} + R_{d_2}}}_{R_d} I_o. \tag{2}$$

Therefore, there is a tradeoff between voltage regulation and load sharing. It is depicted in Fig. 3(b) the bus voltage degradation as a function of α when two sources are feeding a constant current load.

This analysis can be extended to several sources in parallel operating in droop control and connected to the bus by a transmission line, as described in the next topic.

A. Droop With Multiple Sources

The MG structure explored in this paper consists of multiple sources in parallel connected to a common load through transmission lines, as illustrated in Fig. 4. Each source under

droop control is modeled as an ideal voltage source V_i in series with a virtual droop resistance R_{v_i} and each transmission line as a resistance $R_{\mathrm{t_i}}$ in series with an inductance L_{t_i}. The model obtained from the circuit with n sources in Fig. 4 is referred hereinafter as the n-sources model.

The droop and transmission-lines resistances are in series (cf., Fig. 4) and they can be represented by a single equivalent resistance

$$R_{d_i} = R_{v_i} + R_{t_i}. \tag{3}$$

The objective is to control the output resistance of the source, thus the virtual resistance is designed to be $R_{v_i} \gg R_{t_i}$, implying

$$R_{d_i} \approx R_{v_i}. \tag{4}$$

Regarding the same reference voltage V_{ref} for all sources in parallel

$$V_{\mathrm{ref}} = V_1 = V_2 = \cdots = V_n \tag{5}$$

and under the condition

$$\frac{R_{d_1}}{Lt_1} \approx \frac{R_{d_2}}{Lt_2} \approx \cdots \approx \frac{R_{d_n}}{Lt_n} \tag{6}$$

it can be shown that the source subsystem can be approximated by an equivalent resistance R_d and L_d in series with an ideal voltage source, as illustrated in Fig. 4. This equivalent circuit is named *equivalent model* hereinafter.

Most of the systems without droop control ($R_{v_i} = 0$) meet condition (6), because R_{t_i} and L_{t_i} generally keeps a constant ratio no matter the length of the line. However, even using droop control, the equivalent model is near to the n-sources model (n differential equations) if the length of the lines and the power capacity of the sources are similar, which is a common situation in small dc MGs.

To prove that the source subsystem can be approximated by only one differential equation, we use condition (5) in conjunction with the n-sources model. Hence, each transmission line becomes a differential equation given by

$$\begin{aligned}
\frac{di_1}{dt} &= \frac{1}{L_{t_1}}(V_{\mathrm{ref}} - v_{\mathrm{bus}}) - \frac{Rd_1}{L_{t_1}} i_1 \\
\frac{di_2}{dt} &= \frac{1}{L_{t_2}}(V_{\mathrm{ref}} - v_{\mathrm{bus}}) - \frac{Rd_2}{L_{t_2}} i_2 \\
&\vdots \\
\frac{di_n}{dt} &= \frac{1}{L_{t_n}}(V_{\mathrm{ref}} - v_{\mathrm{bus}}) - \frac{R_{d_n}}{L_{t_n}} i_n.
\end{aligned} \tag{7}$$

Furthermore, the total current provided by the sources, denoted by i_{s}, is the sum of the currents of each transmission line

$$i_{\mathrm{s}} = i_1 + i_2 + \cdots + i_n. \tag{8}$$

Therefore, the sum of the n differential equations in (7) is

$$\frac{di_s}{dt} = \frac{d}{dt}\sum_{i=1}^{n} i_i \tag{9}$$

which can be represented as

$$\frac{di_{\mathrm{s}}}{dt} = \left(\sum_{i=1}^{n} \frac{1}{L_{t_i}}\right)(V_{\mathrm{ref}} - v_{\mathrm{bus}}) - \sum_{i=1}^{n} \frac{R_{d_i}}{L_{t_i}} i_i. \tag{10}$$

Substituting condition (6) into (10) results in the approximate differential equation

$$\frac{di_s}{dt} \approx \left(\sum_{i=1}^{n} \frac{1}{L_{t_i}}\right)(V_{\mathrm{ref}} - v_{\mathrm{bus}}) - \frac{R_{d_i}}{L_{t_i}} i_s. \tag{11}$$

To choose the ratio R_{d_i}/L_{t_i} in (11) from all possibilities of condition (6), a good choice is an estimated value given by the ratio of R_{d_μ} and L_{t_μ}

$$\frac{R_{d_i}}{L_{t_i}} \approx \frac{R_{d_\mu}}{L_{t_\mu}} \tag{12}$$

where R_{d_μ} and L_{t_μ} are the arithmetic mean of R_{d_i} and L_{t_i}, respectively

$$R_{d_\mu} = \frac{\sum_{i=1}^{n} R_{d_i}}{n} \quad \text{and} \quad L_{t_\mu} = \frac{\sum_{i=1}^{n} L_{t_i}}{n}. \tag{13}$$

Multiplying both sides of (11) by

$$L_d = \frac{1}{\sum_{i=1}^{n} \frac{1}{L_{t_i}}} \tag{14}$$

and using (12), yields

$$L_d \frac{di_{\mathrm{s}}}{dt} \approx (V_{\mathrm{ref}} - v_{\mathrm{bus}}) - R_{d_\mu} \frac{L_d}{L_{t_\mu}} i_s. \tag{15}$$

Therefore, the equivalent circuit in Fig. 4 is analytically described by (15) when presented as follows:

$$L_d \frac{di_s}{dt} \approx (V_{\mathrm{ref}} - v_{\mathrm{bus}}) - R_d i_{\mathrm{s}} \tag{16}$$

where

$$R_d = R_{d_\mu} \frac{L_d}{L_{t_\mu}}. \tag{17}$$

The aim of the proposed model is to reduce n differential equations from the n transmission lines in parallel to just one, becoming much easier to find the system equilibrium points and their stability, as illustrated in Fig. 4. To prove the effectiveness of this approach, the *complete* output impedance of three sources in parallel, whose internal dynamics of the power converters are considered, is compared to the *equivalent* and the *n-sources model*.

The source V_1 is designed with a virtual resistance $R_{v_1} = 0.2\Omega$ and connected to the bus by the transmission line $T_{L_1} = [28.5\ \mathrm{m}\Omega, 436.5\ \mu\mathrm{H}]$. The parameters values of the sources V_2 and V_3 are related to the source V_1, as described in Table I.

Distributed generation (DG) units were modeled as ideal sources in this paper, but true sources have an internal dynamics that can influence the dynamical behavior of the microgrid. Typically, source's control are based on a cascade control loop structure, with a inner current loop and an outer voltage loop. The inner loop has a minor effect on the microgrid stability, but

TABLE I
PARAMETERS OF V_2 AND V_3 AS A FUNCTION OF V_1.

Sources Parameters	R_{v_2}	R_{v_3}	T_{L_2}	T_{L_3}
Values	$0.5R_{v_1}$	$2R_{v_1}$	$1.4T_{L_1}$	$1.8T_{L_1}$

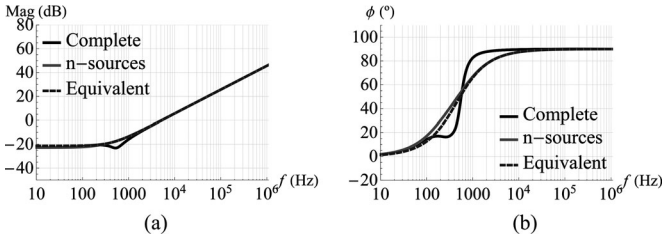

Fig. 5. Bode diagram of the output impedance for the complete, n-sources and equivalent models. (a) Magnitude (dB). (b) Phase (degree).

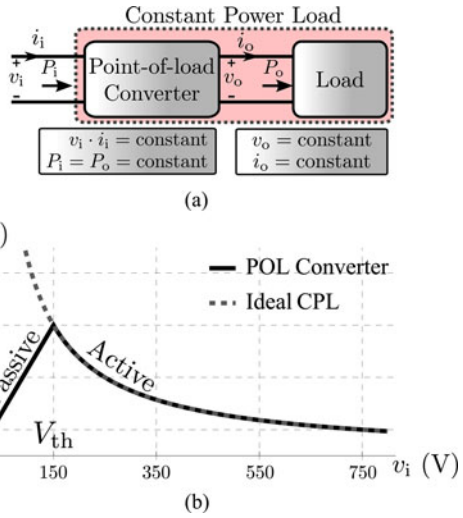

Fig. 6. (a) Block diagram of a POL converter and its input/output voltages and currents. (b) Constant power behavior of a buck converter (380–150 V) driving a 15-Ω resistive load.

the outer voltage loop must have slow dynamics in order to not affect the stability.

Assuming these constraints, the proposed DG units model works properly. In order to validate this model, it is depicted in Fig. 5 the Bode diagrams of the output impedance of the sources (including the transmission lines) corresponding to: 1) complete model that include the internal dynamics of the DG units; 2) n-sources model, and 3) equivalent model. The comparison shows that when the transmission lines are short and have similar lengths with small droop resistance values, the approximation is sufficiently accurate for stability analysis.

Moreover, from the equivalent circuit in Fig. 4, the following two important relations can be obtained:

1) the steady-state voltage bus

$$V_{\rm bus} = V_{\rm ref} - R_d I_o, \quad I_o = I_s; \tag{18}$$

2) and the maximum power that can be transfered to the load

$$P_{\rm max} = \frac{V_{\rm ref}^2}{4R_d}. \tag{19}$$

The second relation is important because there is a type of *instability that is related to the ability to provide the power demanded by the load*. When the load demands more power than $P_{\rm max}$, the bus voltage drops abruptly. This phenomenon is explained in the following sections.

III. DC MICROGRID MODELING

The dc MG evaluated is typical in emergency situations. It operates in island mode without communication to a microgrid central controller or even among the sources, as illustrated in Fig. 1. So, each power converter controller uses only the available local variables. The configuration is composed of the following elements:

1) an intermittent source in maximum power point tracking (MPPT);
2) two batteries of equal capacity (droop control);
3) transmission lines;
4) active loads composed by POL converters;
5) resistive loads;
6) bus capacitance.

The most critical elements to model in a dc MG are the sources, whose behavior depends on their controllers, and loads, especially the POL converters. In the next sections, sources and loads are modeled to support the stability analysis.

A. Constant Power Load

Each load in a dc MG needs a specific voltage level to work properly. This fact forces the system to have POL converters, which are tightly controlled to keep a constant output voltage, as illustrated in Fig. 6(a). It is assumed that the output power of the POL converter is equal to the input power $P_o = P_i$ (hereinafter referred as P). Therefore, POL converters behave as CPLs, because the control action reduces the input current if the input voltage increases and vice versa [22]–[24], [26]. There are two major differences between an ideal CPL and a POL converter. The first one occurs when the input voltage is less or equal than the designed output voltage $V_{\rm th}$ (buck converter with voltage control loop). At this situation, the control saturates the duty cycle, causing the switch to keep closed, consequently, the POL converter becomes a passive load, losing its (CPL) characteristic, as illustrated in Fig. 6(b). Thus, an ideal CPL is represented mathematically as a voltage controlled current source (VCCS)

$$i(v) = \frac{P}{v} \tag{20}$$

and the POL converter as a piecewise (VCCS)

$$i(v) = \begin{cases} \dfrac{P}{v}, & \text{if} \quad v > V_{\rm th} \\ \dfrac{P}{V_{\rm th}^2} v, & \text{if} \quad v \le V_{\rm th}. \end{cases} \tag{21}$$

The second difference occurs at high frequencies. Ideal CPLs responds equally to every frequency, whereas the POL

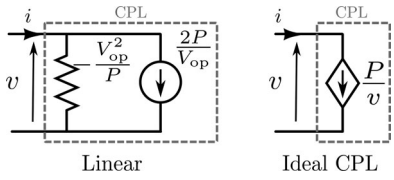

Fig. 7. Linear and ideal CPLs models to represent POL converters.

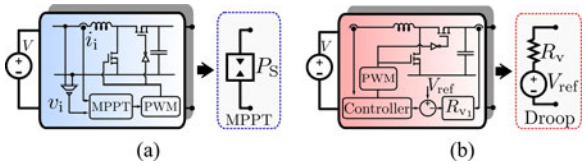

Fig. 8. Sources models. (a) MPPT control. (b) Droop control.

converters are only able to respond to frequencies within the closed-loop bandwidth, although this feature is not modeled in the piecewise function in (21).

Since the ideal CPL model is nonlinear, it is common practice to linearize it in a voltage operating point $V_{\rm op}$

$$i(v) = i(V_{\rm op}) + \frac{\partial i}{\partial v}[v - V_{\rm op}] + O(v^2) \tag{22}$$

$$i(v) \approx 2\frac{P}{V_{\rm op}} + \frac{v}{-\frac{V_{\rm op}^2}{P}}. \tag{23}$$

Such linearization results in a current source in parallel with a negative resistance [15], [16], as illustrated in Fig. 7.

The linear stability analysis is only valid for small deviations around the operating point. Furthermore, it is not able to predict the global behavior of the system, which helps to define a safe operating region. For this reason, throughout this paper, the bus voltage stability is obtained from analytical bifurcation analysis using the ideal CPL model. Afterwards in Section V, a numerical bifurcation analysis is done using the piecewise CPL model (POL converter), as illustrated in Fig. 6(b).

B. Sources

The sources are connected to the MG through power converters, whose control dictates their behavior [4]. Sources under (MPPT) try to maximize the injection of available power to the MG regardless of the network status. Under constant weather conditions, the set PV and power converter can be modeled as (CPS) when viewed by the bus terminals, as illustrated in Fig. 8(a). This means that despite of the variation on the bus voltage, the current provided by the power converter adapts to keep injecting a constant power.

Differently, the batteries under droop control have the role to work cooperatively to keep the bus voltage stable. The resistive output characteristic of the droop controller is modeled as an ideal voltage source in series with a resistance, as illustrated in Fig. 8(b).

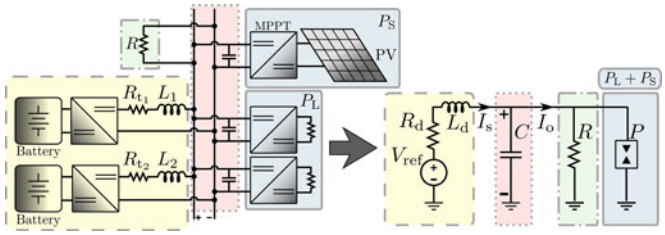

Fig. 9. DC MG circuit setup and its equivalent circuit model.

C. Equivalent Circuit Model and Dynamics of the System

The two batteries in parallel are connected to the bus through transmission lines. Each battery and its power converter are modeled as an ideal voltage source in series with a resistor, as illustrated in Fig. 8(b). A (PV) system operates in MPPT and behaves similarly to a CPL in the sense that it injects the available power to the grid without caring to the system stability. Thus, PVs are considered CPSs and are modeled as depicted in Fig. 8(a). The total power of CPLs (POL converters) on the MG is P_L (positive) and the total power of the CPSs (PVs) is P_S (negative). As CPLs and CPSs behave in the same way, they can be modeled as a lumped CPL that demands an equivalent constant power P given by

$$P = P_L + P_S, \quad P_L \geq 0, \quad \text{and} \quad P_S \leq 0. \tag{24}$$

To analyze the system stability, the sources in parallel under droop control and their transmission lines are modeled as an equivalent voltage source ($V_{\rm ref}$) in series with a resistance R_d and an inductance L_d given by (17) and (14), respectively. The input capacitances of the POL converters and a bank of capacitors connected to the bus are represented by a lumped capacitance C [27], where C is the summation of all capacitances in parallel. Thus, the system to be studied and its model is depicted in Fig. 9, in which P, R, and C correspond to the equivalent CPL, the resistive load, and the lumped capacitance, respectively.

From the equivalent circuit model illustrated in Fig. 9, the dynamics of the dc MG with an ideal CPL can be represented by

$$\begin{aligned} \frac{di_{\rm s}}{dt} &= \frac{1}{L_d}\left(V_{\rm ref} - v_{\rm bus} - R_d i_s\right) \\ \frac{dv_{\rm bus}}{dt} &= \frac{1}{C}\left(i_s - \frac{v_{\rm bus}}{R} - \frac{P}{v_{\rm bus}}\right). \end{aligned} \tag{25}$$

IV. Stability Analysis

The static analysis provides the system equilibrium points, which are obtained by making (25) equals to zero. The two equilibrium points $e_i = [\overline{I}_{s_i}, \overline{V}_{{\rm bus}_i}]$ are

$$\begin{aligned} e_1 &= \left(\frac{V_{\rm ref} - \overline{V}_{{\rm bus}_1}}{R_d}, \frac{RV_{\rm ref} - q}{2(R_d + R)}\right) \\ e_2 &= \left(\frac{V_{\rm ref} - \overline{V}_{{\rm bus}_2}}{R_d}, \frac{RV_{\rm ref} + q}{2(R_d + R)}\right) \end{aligned} \tag{26}$$

where $q = \sqrt{R^2 V_{\rm ref}^2 - 4PRR_d(R_d + R)}$.

Hence, the necessary condition to the existence of equilibrium points is

$$P < \frac{R}{R_d + R}\frac{V_{\text{ref}}^2}{4R_d} = \frac{R}{R_d + R}P_{\max}. \tag{27}$$

The static analysis provides the load conditions to the existence of equilibrium points, but does not specify the stability of such equilibriums. Therefore, a dynamic analysis is necessary to determine which of these equilibriums are stable.

The local stability of typical equilibria is obtained evaluating the Jacobian matrix at each equilibrium point

$$J = \begin{pmatrix} -\dfrac{R_d}{L_d} & -\dfrac{1}{L_d} \\ \dfrac{1}{C} & \dfrac{1}{C}\left(\dfrac{P}{\overline{V}_{\text{bus}}^2} - \dfrac{1}{R}\right) \end{pmatrix} \tag{28}$$

where the stability is determined by the eigenvalues of this matrix.

A. Stability of the First Equilibrium $e_1 = (\overline{I}_{s_1}, \overline{V}_{\text{bus}_1})$

The Jacobian matrix in (28) evaluated at e_1 has always a determinant $\Delta < 0$. In planar systems, this means the existence of two eigenvalues with opposite signs. Thus, it is a *saddle equilibrium*, and consequently, always unstable.

B. Stability of the Second Equilibrium $e_2 = (\overline{I}_{s_2}, \overline{V}_{\text{bus}_2})$

The second equilibrium point is stable when the trace of (28) is less than zero ($\tau < 0$) and the determinant greater than zero ($\Delta > 0$). Solving these inequalities results in following two cases that guarantees the stability of e_2:

1) $C > \frac{L_d}{R_d^2}$, the system is stable when

$$P < P_I = \frac{RV_{\text{ref}}^2}{4R_d(R_d + R)} = \frac{R}{R_d + R}P_{\max}; \tag{29}$$

2) $C \leq \frac{L_d}{R_d^2}$, the system is stable when

$$P < P_{II} = \frac{L_d R V_{\text{ref}}^2 (CR_dR + L_d)}{\left(CR_d^2R + L_d(2R_d + R)\right)^2}. \tag{30}$$

When the lumped capacitance C belongs to case 1, the equilibrium point is stable for any value of P within the equilibrium existence condition described in (27). *The case 1 system has only one type of instability related to the incapacity of the system to provide the power demanded by the load at $P = P_I$.*

On the other hand, if C belongs to case 2, the equilibrium is stable only over a smaller range of load values ($P < P_{\text{II}}$). In this case, *the instability occurs at $P = P_{\text{II}}$ due to the interaction between the load and source subsystems*.

Thus, in a case 2 system, if P is increased until it reaches P_{II}, a subcritical Hopf bifurcation (*H*) occurs and the equilibrium becomes unstable [28]. It is illustrated in Fig. 10 all possible e_1 and e_2 equilibrium points when varying the parameter P for a case 2 system with two sources in parallel with the parameters described in Table II.

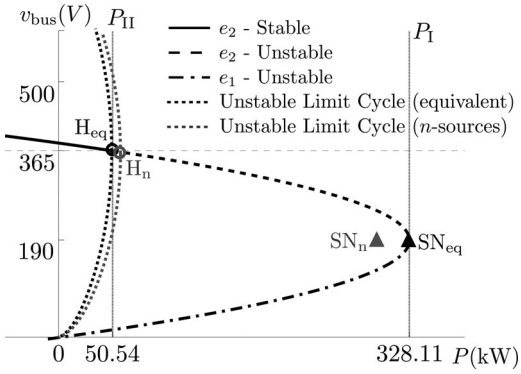

Fig. 10. Bifurcation diagram of the equilibrium points varying P with a fixed $R = 500\,\Omega$ of a case 2 system. The points H_{eq} and H_{n} represent the Hopf bifurcation of the equivalent and n-sources models, respectively. The same notation is used for the saddle-node points, SN_{eq} and SN_{n}.

TABLE II
CIRCUIT SIMULATION PARAMETERS OF A 380-V DC MICROGRID

	$R_v\,(\Omega)$	$R_t\,(\omega)$	$L_t\,(\mu H)$	$C(mF)$	$R(\Omega)$	P (W)
DG 1	0.2	28.5	436.5	1	500	Variable
DG 2	0.2	57	873			

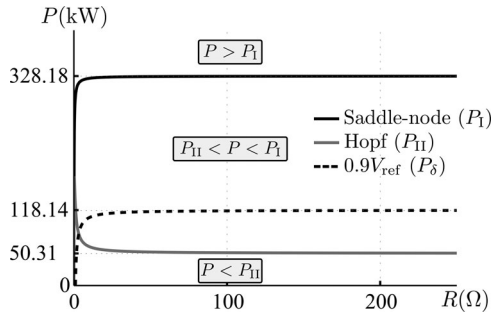

Fig. 11. Stability regions for any combination of CPL and resistive loads of a case 2 system using the equivalent model.

The system has a nominal voltage of 380 V and the CPL is a POL buck converter (380–150 V) driving a variable resistance that should be supplied with 150 V. This setup is designed to be a case 2 system with a $R_d = 0.11\ \Omega$ and $L_d = 291\ \mu$H.

The equilibrium e_2 is unstable for any value of P higher than P_{II} and lower than P_{I} (cf., Fig. 10). There are no equilibrium points for P values above P_{I}, because a saddle-node bifurcation (SN_{eq}) [28] occurs when e_1 and e_2 meet each other at P_{I} and both equilibrium points disappear. It is illustrated in Fig. 11 a diagram in (R, P) plane representing all the load conditions (combinations of R and P) for the system described in Table II. The continuous black and gray lines are P_{I} and P_{II}, respectively. When the system load is under the gray line, the equilibrium e_2 is stable, otherwise it is unstable. At the gray line, a subcritical Hopf bifurcation (H_{eq}) and at the black line a saddle-node bifurcation (SN_{eq}), i.e., above this line there are no equilibrium points.

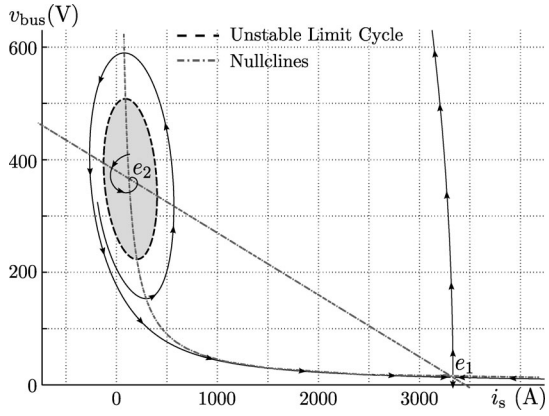

Fig. 12. Phase portrait of a case 2 system when $P < P_{\rm II}$.

A typical phase portrait for a case 2 system when $P < P_{\rm II}$ (e_2 stable) is illustrated in Fig. 12. There is always an unstable limit cycle around the stable equilibrium point, which defines the stability region (shaded area). Therefore, the state always returns to the equilibrium point for any disturbance that shifts the state from the equilibrium point without crossing the unstable limit cycle. The shaded area decreases as P approaches $P_{\rm II}$.

Stability is not the only concern when designing an MG, all the loads need a bus voltage regulated within an acceptable range to work properly. In this scenario, P and R should be limited to keep the voltage within a tolerance range δ specified as a percentage of the reference value $V_{\rm ref}$. So, the voltage bus restriction is given by

$$\overline{V}_{\rm bus} \geq \delta V_{\rm ref}, \quad \text{with} \quad 0.5 < \delta < 1. \tag{31}$$

The quota of P and R loads that can be connected to a droop-controlled system without exceeding the voltage drop limit is obtained by substituting the voltage of equilibrium point e_2 into (31), which results in

$$P < P_\delta = \frac{\delta V_{\rm ref}^2 [R - \delta(R_d + R)]}{R_d R}. \tag{32}$$

This inequality defines the load allowed to keep the bus voltage inside the tolerance range. It is illustrated in Fig. 11 a black dashed line that limits the region for a tolerance range defined as 90% ($\delta = 0.9$) of 380 V. Thus, the tolerance on the bus voltage drop may become more restrictive than the stability constraint.

Cases 1 and 2 show that if R_d is increased, the lumped capacitance necessary to keep the system stable decreases. The relation among C, L_d, and R_d presented in cases 1 and 2 allows to define the capacitance required for stability not only in a operating point, but in the entire voltage range to a given load. Based on this analysis, a design guideline to obtain a stable dc MG is described.

C. Designing a Stable DC MG

Based on the preceding analysis, the steps for obtaining a stable DC MG are described below and presented via a flowchart in Fig. 13.

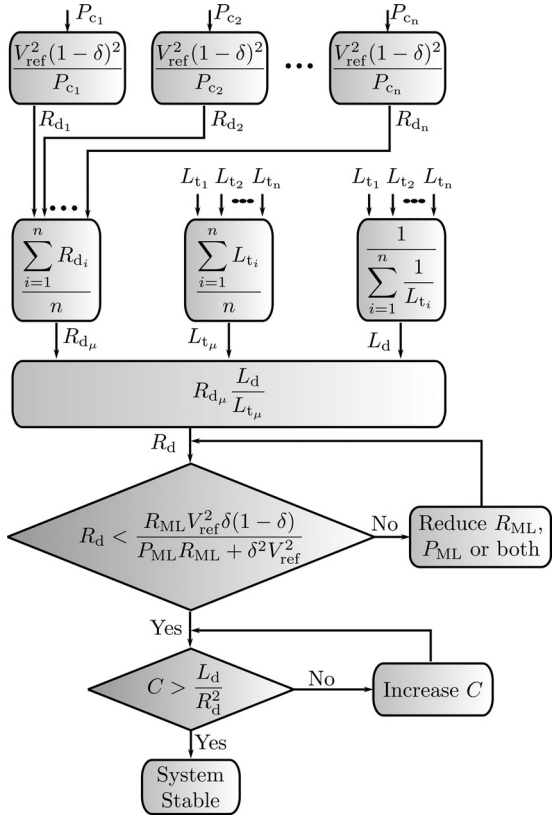

Fig. 13. Flowchart to design a stable dc microgrid.

1) obtain the power capacities of each droop-controlled source (P_{c_i});
2) set the desired tolerance range δ and the reference voltage $V_{\rm ref}$;
3) Set the maximum constant power and the resistive load allowed in the MG, $P_{\rm ML}$, and $R_{\rm ML}$, respectively. As the resistance is reduced more power is required, so $P_{\rm ML}$ is the maximum value of P and $R_{\rm ML}$ is the minimum value of R.

From the power capacities the droop resistance of each power source (R_{d_i}) is obtained. This method assumes $R_{d_i} \gg R_{t_i}$, as explained in (3). Using the values of R_{d_i} and L_{t_i}, it is obtained the value of R_d, which should meet the specification of voltage drop in (32). Once the power demanded by the resistive and constant power loads is met, the capacitance value to keep the system stable is adjusted.

V. Simulation Results

In this section, simulation results are shown to validate the stability analysis under load variations. Two sources in parallel interfaced by dc–dc boost converters are connected through transmission lines to a bus with resistive and CPL loads, as illustrated in Fig. 14. The sources have the same capacity and are under droop control (R_v) with the parameters given by Table II.

The bus voltage has a nominal value of 380 V and the CPL load is a POL buck converter (380–150 V) driving a variable

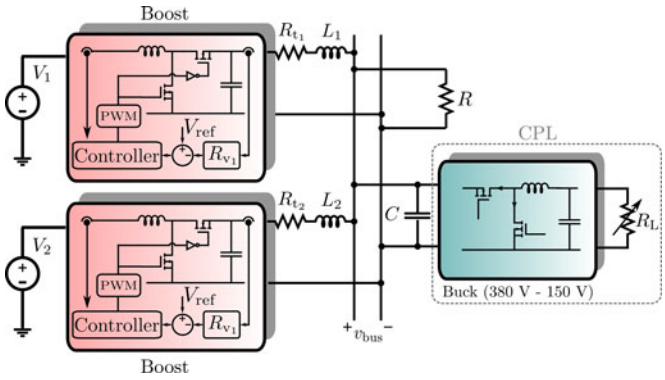

Fig. 14. Circuit used in the simulation to validate the stability analysis of a 380-V island dc microgrid.

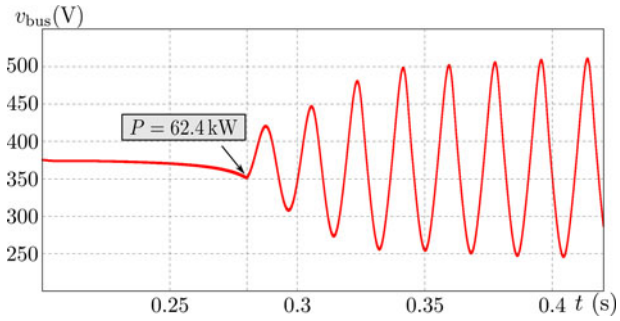

Fig. 15. Point where the bus voltage under CPL variation starts to oscillate (after the Hopf bifurcation).

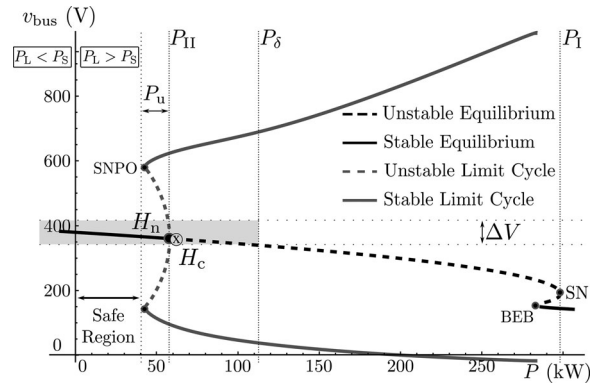

Fig. 16. Bifurcation diagram of the system $P \times V_{\rm bus}$ (POL converter), where $P = P_S + P_L$. The H_c and H_n represent the Hopf bifurcations obtained from the circuit of Fig. 14 and the n-sources model, respectively.

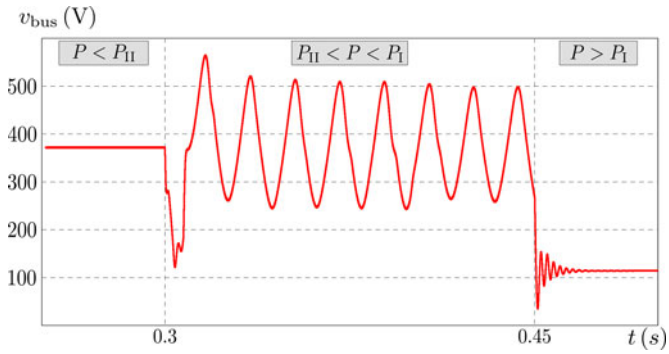

Fig. 17. Time response of the simulated circuit using three different CPLs.

resistance R_L. This setup is designed to be a case 2 system with $R_d = 0.11\ \Omega$ and $L_d = 291\ \mu$H. Using these values in (30), it is possible to conclude that the system is stable for $P < P_{\rm II} = 49.72$ kW, where a Hopf bifurcation occurs making the system oscillate.

To validate the stability analysis, CPL variations are imposed to the system and compared to the mathematical analysis. The system is evaluated by varying the resistance R_L driven by the POL converter, which is equivalent to a CPL variation (P). The resistance is decreased in very small steps from $10\ \Omega$ until the system becomes unstable. This method is chosen because the stability analysis is local and high step variations can make the state, even for a stable equilibrium, leave the equilibrium region of attraction and turn the system unstable. It is illustrated in Fig. 15 the bus voltage behavior when the load power P is increased in small steps. When P reaches 62.4 kW, a subcritical Hopf bifurcation occurs and the system starts to oscillate after this critical point.

This oscillation is only possible in case 2 systems, because there is a subcritical Hopf bifurcation before it reaches the maximum power that can be transferred to the load. The same results are depicted over a bifurcation diagram (obtained using AUTO software [29]) of the bus voltage as a function of the P parameter in Fig. 16. The diagram is built from the n-sources model using the POL converter model of (21) (cf., Fig. 6).

It is noteworthy from the Fig. 16 that the Hopf bifurcation point predicted by the equivalent model ($P_{\rm II} = 49.72\ kW$) occurs for a smaller P than that obtained for the n-sources model (H_n) and the complete circuit (H_c) illustrated in Fig. 14. The difference between the Hopf bifurcation point predicted using the equivalent model and the n-sources model is due to the approximation used to represent the n-sources with only one equivalent source. For the complete circuit, this difference occurs for two main reasons. The first one, besides the approximation by a single source, the equivalent model disregards the internal dynamics of the converter. The second reason, and no less important, is the effect of conservative modeling applied to POL converters, which are considered ideal CPLs. POL converters do not have CPL characteristic over the whole spectrum of frequencies, and consequently, they are much more stable, as described in Section III.

Note that the diagram of Fig. 16 has four bifurcations and three main regions. The main dynamic behaviors in time domain of $v_{\rm bus}$ relative to these regions can be seen in Fig. 17. The saddle-node bifurcation of periodic orbits (SNPO) occurs due to the passive region present in POL converters (cf., Fig. 6), which give rise to a stable limit cycle.

At high P values there are two main equilibria bifurcations, (SN) and boundary equilibrium bifurcation (BEB)[30] (see Fig. 16). The first one is the maximum power which the MG can

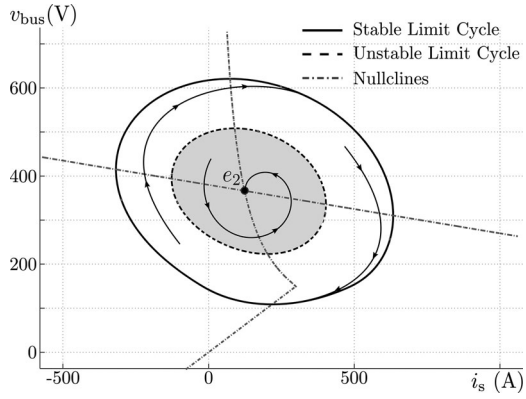

Fig. 18. Phase portrait of the system using the POL converter model for a P inside the stable (although unsafe) region $P_{\rm u}$.

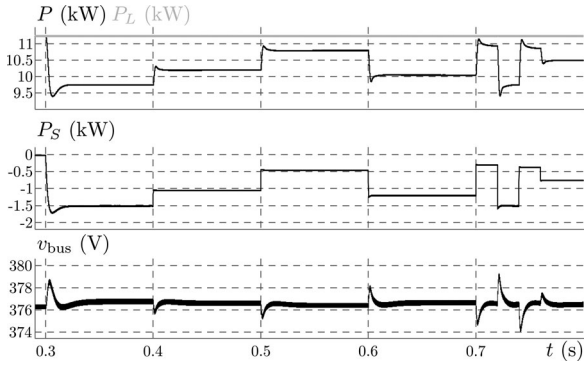

Fig. 19. Bus voltage under intermittent power sources.

provide to the CPL; the second one shows up due to the discontinuity from the POL converter model, where two equilibria, one from the passive region and the other from the active region collide on the boundary ($V_{\rm th}$). Therefore, BEB occurs when the bus voltage drops below the $V_{\rm th}$ (cf. Fig. 6) and $P > P_{\rm BEB}$. The BEB bifurcation gives rise to a stable equilibrium point, which is obtained experimentally in the next section.

It can be stated based on the bifurcation diagram of Fig. 16 that the values of P inside the $P_{\rm u}$ region, although the system is locally stable, it may become unstable when the bus voltage is disturbed and cross the unstable limit cycle. If this happens, the bus voltage is attracted by the stable limit cycle and start to oscillate. To illustrate this behavior a phase portrait of the system for a P within the $P_{\rm u}$ region is depicted in Fig. 18. Therefore, the safe region is composed by all values of P located to the left of the SNPO bifurcation point. For instance, when an intermittent source (P_S) is connected to the bus and the total power ($P = P_S + P_L$) is in the safe region, the system stability is not affected, as illustrated in Fig. 19. As a consequence of this analysis, microgrids should be designed to operate in the safe region regardless the intermittent sources, since the power provided by them have a stabilizing effect.

VI. Experimental Results

The aim of this section is to validate only the saddle-node bifurcation (SN) where two equilibria collide and the bus voltage system drops very fast to a stable equilibrium point that undergoes from BEB. In order to show this behavior, a simple setup composed by two sources of 24 V in parallel with high output resistances $R_{d_1} = 20\ \Omega$ and $R_{d_2} = 33\ \Omega$ were implemented. These resistances emulate two sources under droop control. The load is composed by a resistance $R = 133\ \Omega$ and a buck converter (24–8 V) driving a variable resistance, as illustrated in Fig. 20.

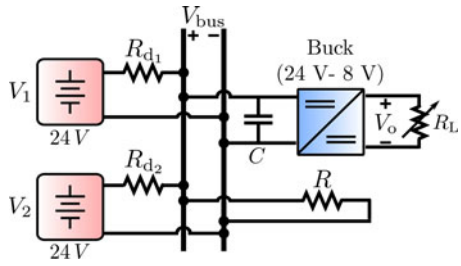

Fig. 20. Experimental circuit setup to validate the bus voltage stability analysis.

TABLE III
Measured Values of the Experimental Set of Fig. 20

CPL Steps	Initial	Step 1	Step 2
P (W)	5.39	6.74	13.06
$P_{\rm Res}$ (W)	2.45	2.02	–
$P_{\rm Total}$ (W)	7.84	8.76	–
$V_{\rm bus}$ (V)	18.04	16.4	7.04
V_o (V)	7.96	7.96	5.76

This simple experimental setup emulates a system where the capacitance is much larger than the inductance, characterizing a case 1 system, which does not have the subcritical Hopf bifurcation. The experimental setup does not have any transmission-line inductances, $R_d = 12.45\ \Omega$ (parallel of the droop resistances), and consequently, the maximum power that can be transfered to the load is $P_{\rm I} = 10.57$ W (SN).

Thus, if the POL converter demands more power than the sources are capable to provide, a saddle-node bifurcation (SN) occurs and the system collapses. To show how this happens experimentally, first the buck converter feeds a resistive load of $47\ \Omega$ that draws 1.35 W from the sources. The buck output resistance is switched in two steps until the power demanded by the system exceeds $P_{\rm I}$. The CPL power P, the bus voltage $V_{\rm bus}$, and the power consumed by the resistive load $P_{\rm res}$ are described in Table III. The bifurcation diagram corresponding to the experimental setup is depicted in Fig. 21(a), whereas the bus and the buck output voltages time response are illustrated in Fig. 21(b) and (c).

When step 2 occurs, the power required by the CPL exceeds the power $P_{\rm I}$ and the system collapses. The bus voltage drops very fast and the buck converter tries to provide the power demanded by the load modifying the duty cycle for increasingly higher values, until the duty-cycle value saturates, forcing the switch to remain closed. At this point, the power converter loses its constant power characteristic and starts to behave passively

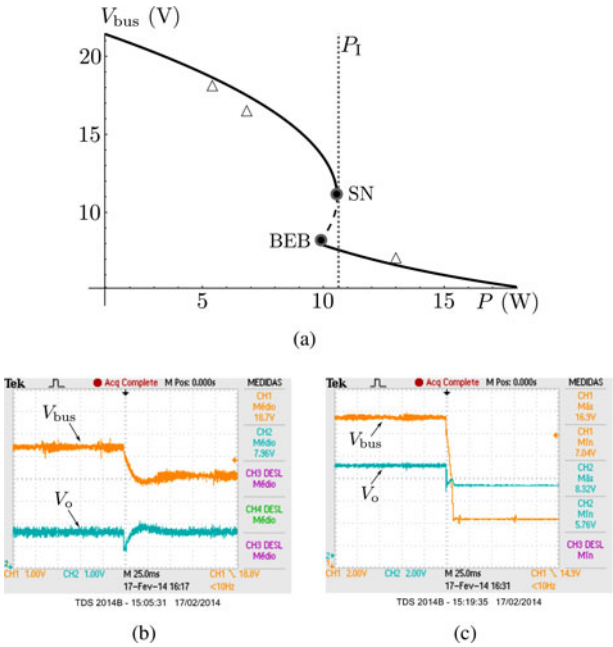

Fig. 21. (a) Bifurcation diagram of the experimental setup, where the △ markers stand for the experimental values of the bus voltage; (b) Step 1—CPL variation from 5.39 to 6.74 W; (c) Step 2—CPL variation from 6.74 to 13.06 W. The power demanded after this step exceeds the SN bifurcation and the system collapses.

as an *RLC* circuit, as illustrated in Fig. 21(c). That is why the system finds a stable equilibrium point after the SN, as expected by the bifurcation diagram in Fig. 21(a). This stable equilibrium is represented by the black continuous line after the BEB.

VII. Conclusion

DC MGs are emerging as distributed generation solutions to some applications that need efficiency and reliability. Under this perspective, this paper has addressed a simplified model to reduce the complexity of the nonlinear stability analysis for small dc microgrids under droop control without communication. The proposed equivalent model keeps the qualitative behavior of the system while reducing the complexity of the stability analysis.

The nonlinear analysis based on the bifurcation theory give us some relations among the MG parameters, which allow us to determine the qualitative behavior of the system. In this sense, bifurcation diagrams presented along this paper offers a design guideline to build reliable MGs based on safe operation regions.

Acknowledgment

The authors would like to thank Dr. M. L. Heldwein and his collaborators from the Power Electronics Institute (INEP), Federal University of Santa Catarina, Brazil, for their constant support and constructive suggestions.

References

[1] F. Blaabjerg, Z. Chen, and S. Kjaer, "Power electronics as efficient interface in dispersed power generation systems," *IEEE Trans. Power Electron.*, vol. 19, no. 5, pp. 1184–1194, Sep. 2004.

[2] H. Kakigano, Y. Miura, and T. Ise, "Low-voltage bipolar-type dc microgrid for super high quality distribution," *IEEE Trans. Power Electron.*, vol. 25, no. 12, pp. 3066–3075, Dec. 2010.

[3] D. Boroyevich, I. Cvetkovic, D. Dong, R. Burgos, F. Wang, and F. Lee, "Future electronic power distribution systems a contemplative view," in *Proc. 12th Int. Conf. Optimization Electr. Electron. Equipment*, May 2010, pp. 1369–1380.

[4] D. Chen, L. Xu, and L. Yao, "DC voltage variation based autonomous control of dc microgrids," *IEEE Trans. Power Del.*, vol. 28, no. 2, pp. 637–648, Apr. 2013.

[5] J. Guerrero, J. Vasquez, J. Matas, L. de Vicuna, and M. Castilla, "Hierarchical control of droop-controlled ac and dc microgrids a general approach toward standardization," *IEEE Trans. Ind. Electron.*, vol. 58, no. 1, pp. 158 –172, Jan. 2011.

[6] S. Anand, B. G. Fernandes, and M. Guerrero, "Distributed control to ensure proportional load sharing and improve voltage regulation in low-voltage dc microgrids," *IEEE Trans. Power Electron.*, vol. 28, no. 4, pp. 1900–1913, Apr. 2013.

[7] X. Lu, J. Guerrero, K. Sun, and J. Vasquez, "An improved droop control method for dc microgrids based on low bandwidth communication with dc bus voltage restoration and enhanced current sharing accuracy," *IEEE Trans. Power Electron.*, vol. 29, no. 4, pp. 1800–1812, Apr. 2014.

[8] T. Dragicevic, J. Guerrero, J. Vasquez, and D. Skrlec, "Supervisory control of an adaptive-droop regulated dc microgrid with battery management capability," *IEEE Trans. Power Electron.*, vol. 29, no. 2, pp. 695–706, Feb. 2014.

[9] A. Rahimi and A. Emadi, "Active damping in dc/dc power electronic converters: A novel method to overcome the problems of constant power loads," *IEEE Trans. Ind. Electron.*, vol. 56, no. 5, pp. 1428 –1439, May 2009.

[10] P. Liutanakul, A.-B. Awan, S. Pierfederici, B. Nahid-Mobarakeh, and F. Meibody-Tabar, "Linear stabilization of a dc bus supplying a constant power load: A general design approach," *IEEE Trans. Power Electron.*, vol. 25, no. 2, pp. 475–488, Feb. 2010.

[11] R. Middlebrook and S. Cuk, "Input filter considerations in design and application of switching regulators," in *Proc. IEEE Ind. Appl. Annu. Meeting*, Chicago, IL, USA, 1976.

[12] B. Cho, J. Lee, and F. Lee, "Large-signal stability analysis of spacecraft power processing systems," *IEEE Trans. Power Electron.*, vol. 5, no. 1, pp. 110 –116, Jan. 1990.

[13] C. Wildrick, F. Lee, B. Cho, and B. Choi, "A method of defining the load impedance specification for a stable distributed power system," *IEEE Trans. Power Electron.*, vol. 10, no. 3, pp. 280–285, May 1995.

[14] J. Liu, X. Feng, F. Lee, and D. Borojevich, "Stability margin monitoring for dc distributed power systems via perturbation approaches," *IEEE Trans. Power Electron.*, vol. 18, no. 6, pp. 1254–1261, Nov. 2003.

[15] C. Rivetta, G. Williamson, and A. Emadi, "Constant power loads and negative impedance instability in sea and undersea vehicles: statement of the problem and comprehensive large-signal solution," in *Proc. IEEE Electr. Ship Technol. Symp.*, Jul. 2005, pp. 313–320.

[16] A. Emadi, A. Khaligh, C. Rivetta, and G. Williamson, "Constant power loads and negative impedance instability in automotive systems: definition, modeling, stability, and control of power electronic converters and motor drives," *IEEE Trans. Veh. Technol.*, vol. 55, no. 4, pp. 1112–1125, Jul. 2006.

[17] A. Radwan and Y.-R. Mohamed, "Linear active stabilization of converter-dominated dc microgrids," *IEEE Trans. Smart Grid*, vol. 3, no. 1, pp. 203–216, Mar. 2012.

[18] A. Radwan and Y. Mohamed, "Assessment and mitigation of interaction dynamics in hybrid ac/dc distribution generation systems," *IEEE Trans. Smart Grid*, vol. 3, no. 3, pp. 1382–1393, Sep. 2012.

[19] X. Liu, A. Forsyth, and A. Cross, "Negative input-resistance compensator for a constant power load," *IEEE Trans. Ind. Electron.*, vol. 54, no. 6, pp. 3188–3196, Dec. 2007.

[20] J. Schonberger, R. Duke, and S. D. Round, "DC bus signalling: A distributed control strategy for a hybrid renewable nanogrid," *IEEE Trans. Ind. Electron.*, vol. 53, no. 5, pp. 1453–1460, Oct. 2006.

[21] K. Sun, L. Zhang, Y. Xing, and J. Guerrero, "A distributed control strategy based on dc bus signaling for modular photovoltaic generation systems with battery energy storage," *IEEE Trans. Power Electron.*, vol. 26, no. 10, pp. 3032–3045, Oct. 2011.

[22] A. Kwasinski and C. Onwuchekwa, "Dynamic behavior and stabilization of dc micro-grids with instantaneous constant-power loads," *IEEE Trans. Power Electron.*, vol. 26, no. 3, pp. 822–834, Nov. 2010.

[23] A. P. N. Tahim, D. J. Pagano, M. L. Heldwein, and E. Ponce, "Control of interconnected power electronic converters in dc distribution systems," in *Proc. 11th Brazilian Power Electron. Conf.*, 2011, pp. 269–274.
[24] A. P. N. Tahim, D. J. Pagano, and E. Ponce, "Nonlinear control of dc-dc bidirectional converters in stand-alone dc microgrids," in *Proc. IEEE 51st Annual Conf. Decision Control.*, Dec. 2012, pp. 3068 –3073.
[25] W. Du, J. Zhang, Y. Zhang, and Z. Qian, "Stability criterion for cascaded system with constant power load," *IEEE Trans. Power Electron.*, vol. 28, no. 4, pp. 1843–1851, Apr. 2013.
[26] A. Emadi, A. Khaligh, C. Rivetta, and G. Williamson, "Constant power loads and negative impedance instability in automotive systems: definition, modeling, stability, and control of power electronic converters and motor drives," *IEEE Trans. Veh. Technol.*, vol. 55, no. 4, pp. 1112–1125, Jul. 2006.
[27] L. Xu and D. Chen, "Control and operation of a dc microgrid with variable generation and energy storage," *IEEE Trans. Power Del.*, vol. 26, no. 4, pp. 2513–2522, Oct. 2011.
[28] J. Guckenheimer and P. Holmes, *Nonlinear Oscillations, Dynamical Systems and Bifurcations of Vector Fields*. New York, NY, USA: Springer, 1983.
[29] E. J. Doedel, A. R. Champneys, T. F. Fairgrieve, Y. A. Kuznetsov, B. Sandstede, and X. Wang, "Auto 97: Continuation and bifurcation software for ordinary differential equations (with Homcont)," 1998. http://indy.cs.concordia.ca/auto/
[30] D. Pagano, E. Ponce, and F. Torres, "On double boundary equilibrium bifurcations in piecewise smooth planar systems," *Qualitative Theory Dynam. Syst.*, vol. 10, no. 2, pp. 277–301, 2011.

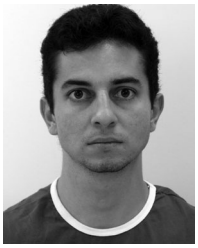

André Pires Nóbrega Tahim (S'12) was born in Serrinha-Bahia, Brazil, in 1981. He received the B.Sc. degree in electrical engineering from the Federal University of Bahia (UFBA), Salvador, Brazil, in 2004, and the M.Eng. degree in electrical engineering from the Federal University of Santa Catarina, Florianópolis, Brazil, in 2009, where he is currently working toward the D.Eng. degree in control and automation engineering.

His current research interests include power electronics, microgrids, nonlinear control, and their applications.

Daniel J. Pagano (M'09) was born in La Plata, Argentine, in 1961. He received the B.Sc. degree in telecommunications engineering from the National University of La Plata, La Plata, Argentine, in 1985, the M.Sc. degree in electrical engineering from the Federal University of Santa Catarina, Florianópolis, Brazil, in 1989, and the Ph.D. degree in Robotics, Automation and Electronics from the University of Seville, Sevilla, Spain, in 1999.

He is currently a Professor at the Department of Automation and Systems, Federal University of Santa Catarina. His main research interests include nonlinear dynamical systems, bifurcation analysis, nonlinear control, power electronics, and microgrids and their applications.

Eduardo Lenz (S'10) received the B.Sc. and M.Sc. degrees in electrical engineering from the Federal University of Ceará, Fortaleza, Brazil, in 2008 and 2011, respectively. He is currently working toward the Ph.D. degree in control and automation engineering with the Federal University of Santa Catarina, Florianópolis, Brazil.

His main research interests are nonlinear control applied to power electronics, adaptive control, nonlinear dynamics, bifurcation analysis, and electromagnetic fields.

Vinicius Stramosk (S'09) received the B.S. and M.S. degrees in control and automation engineering from the Federal University of Santa Catarina, Florianópolis, Brazil, in 2011 and 2014, respectively.

His main research interests include control strategies for microgrids, nonlinear control, and power electronics.